communications physics

A Nature Portfolio journal

Article

https://doi.org/10.1038/s42005-026-02566-y

Thermodynamic anomalies in overdamped systems with time-dependent temperature

Shakul Awasthi [1], Hyunggyu Park [2] & Jae Sung Lee [1,2] ✉

One of the objectives in investigating small stochastic systems is the development of micrometer-sized engines and the understanding of their thermodynamics. However, the main mathematical tool used for this purpose, the overdamped approximation, has a critical limitation: it fails to capture the thermodynamics when the temperature varies over time. We show that heat dissipation and entropy production computed under this approximation deviate from their true values, and these discrepancies are termed thermodynamic anomalies. To address this, we analytically derive expressions for these anomalies in the presence of a general time-varying temperature. A key feature of the result is that high viscosity and small mass, though both leading to the same overdamped equations, yield different anomaly relations. Our results have broad implications, particularly for accurately evaluating engine efficiency in overdamped environments with time-varying temperatures and provide a method for estimating the kinetic energy of an overdamped system.

Recent studies on stochastic systems have driven significant advancements in thermodynamics at the microscopic scale. These advancements have enabled the miniaturization of heat engines to a microscopic level[1–5], particularly using a single colloidal particle in overdamped environments[2,6–8]. The dynamics of such small systems are often analyzed by considering only their position trajectories while neglecting velocity variables. This simplification is justified because experimental systems are typically overdamped, meaning that velocity relaxes to equilibrium much faster than position dynamics in environments with high viscosity or negligible inertia effects. Due to its simplicity in mathematical handling, this overdamped approximation is widely employed to describe the dynamics observed in mesoscopic experiments involving typical fluids. In addition, this approximation is, in some sense, inevitable, as accurately measuring velocity in overdamped systems is challenging due to its rapid relaxation.

However, the overdamped approximation does not always guarantee accurate estimation of thermodynamic quantities, such as heat and entropy production (EP), even in environments with high viscosity or small mass. One example is a system with a position-dependent temperature[9–16]. In such systems, EP calculated under the overdamped approximation differs from that obtained using the full underdamped formalism, which explicitly accounts for the velocity variable[11]. The difference between the two EPs is attributed to the symmetry breaking of time and velocity. As shown in this example, the finite discrepancy between thermodynamic quantities calculated under the overdamped approximation and the underdamped formulation is referred to as a *thermodynamic anomaly*[11].

Therefore, thermodynamic anomalies play a crucial role in calculating thermodynamic quantities when velocity measurement is challenging. Despite their importance, there has been no systematic study on thermodynamic anomalies induced by time-dependent temperature, aside from several reports on specific systems[17–19]. Investigating these anomalies in systems with time-varying temperature is essential due to their broad applicability in both theoretical and experimental contexts. This is particularly relevant in the field of microscopic heat engines, where temperature varies periodically over time. Indeed, numerous microscopic heat engine models have been proposed over the past two decades[17,20–30]. If these anomalies can be properly evaluated and accounted for, thermodynamic quantities related to such engines might be accurately calculated using the simpler overdamped formalism, without requiring velocity measurements.

Here, we explicitly calculate the thermodynamic anomalies in heat and EP for systems with general time-varying temperature. Our results demonstrate that the two conditions, high viscosity and small mass, result in different thermodynamic anomaly relations, though both leading to the same overdamped dynamics. Moreover, we also find general anomaly relations in between the two conditions by introducing the two-parameter Brinkman's hierarchy method. This indicates that accurately estimating thermodynamic quantities in overdamped systems with time-varying temperatures requires understanding the underlying mechanism that leads

[1]School of Physics, Korea Institute for Advanced Study, Seoul, Korea. [2]Quantum Universe Center, Korea Institute for Advanced Study, Seoul, Korea.
✉e-mail: jslee@kias.re.kr

to the overdamped regime. Through numerical examples, we demonstrate that heat, efficiency of a heat engine, and kinetic energy can be accurately estimated in overdamped environments without the need for intricate velocity measurements, even when the temperature varies relatively quickly.

Results

Setup

Consider a one-dimensional Brownian particle of mass m immersed in a reservoir with a time-varying temperature $T(t)$. The position and velocity of the particle at time t are denoted by x_t and v_t, respectively. The motion of the particle is described by a stochastic differential equation known as the underdamped Langevin equation, given by

$$\dot{x}_t = v_t, \;\; m\dot{v}_t = f(x_t, \lambda_t) - \gamma v_t + \eta_t \,, \tag{1}$$

where $f(x_t, \lambda_t)$ denotes an external force applied on the particle, λ_t represents a given time-dependent protocol, and γ is the viscous coefficient. η_t denotes the thermal Gaussian-white noise characterized by a zero mean and the autocorrelation $\langle \eta_t \eta_{t'} \rangle = 2\gamma T(t)\delta(t-t')$ with the Boltzmann constant set to $k_B = 1$. Both conservative and nonconservative forces can be included in $f(x_t, \lambda_t)$. The probability distribution $P_{\rm ud}(x, v, t)$ for the stochastic variables x_t and v_t at time t is governed by the following Fokker-Planck (FP) equation[31]:

$$\partial_t P_{\rm ud}(x, v, t) = \mathcal{L}_{\rm ud} P_{\rm ud}(x, v, t) \,, \tag{2}$$

where the underdamped FP operator $\mathcal{L}_{\rm ud}$ is defined as

$$\mathscr{L}_{\rm ud} := -\partial_x v - \frac{1}{m}\partial_v \left[f(x,\lambda) - \gamma v - \frac{\gamma T(t)}{m}\partial_v \right] . \tag{3}$$

We now turn our attention to the thermodynamics of the system. According to the first law of thermodynamics at the trajectory level[32], the mean value of heat rate $\dot{Q}$ in the underdamped system is given by

$$\langle \dot{Q} \rangle_{\rm ud} = -\langle \gamma v^2 \rangle_{\rm ud} + \langle v \circ \eta \rangle_{\rm ud} \,, \tag{4}$$

where the symbol $\circ$ denotes the Stratonovich product and $\langle \cdots \rangle_{\rm ud}$ represents the ensemble average taken over the probability distribution $P_{\rm ud}(x, v, t)$. The expression of the heat rate in Eq. (4) is equivalent to

$$\langle \dot{Q} \rangle_{\rm ud} = \int_{-\infty}^{\infty} dx \int_{-\infty}^{\infty} dv \, m v J^{\rm irr}_{\rm ud}(x, v, t) \,, \tag{5}$$

where $J^{\rm irr}_{\rm ud}(x, v, t)$ is defined as

$$J^{\rm irr}_{\rm ud}(x, v, t) \equiv \left(-\frac{\gamma v}{m} - \frac{\gamma T(t)}{m^2}\partial_v \right) P_{\rm ud}(x, v, t) \,. \tag{6}$$

Then, the rate of total EP can be expressed using $J^{\rm irr}_{\rm ud}(x, v, t)$ as follows[33–36]:

$$\langle \dot{S}_{\rm tot} \rangle_{\rm ud} = \int_{-\infty}^{\infty} dx \int_{-\infty}^{\infty} dv \, \frac{(m J^{\rm irr}_{\rm ud})^2}{\gamma T(t) P_{\rm ud}} \,. \tag{7}$$

Time scales and overdamped equations

There are four characteristic time scales in this setup: (i) the velocity relaxation time $\tau_{\rm r} \equiv m/\gamma$, (ii) the time interval between two consecutive observations of the system $\tau_{\rm obs}$, (iii) the time scale of temperature variation $\tau_{\rm tmp}$, and (iv) the typical time scale of x-variable (overdamped) dynamics $\tau_{\rm od}$. When the condition $\tau_{\rm r}/\tau_{\rm obs} \ll 1$ is satisfied, the velocity is always relaxed to equilibrium for any observation time. If the temperature is time-independent, the overdamped description using only the x variable is valid under the single condition $\tau_{\rm r}/\tau_{\rm obs} \ll 1$. However, if the temperature is time-dependent, the overdamped approximation also depends on $\tau_{\rm tmp}$: for example, when $\tau_{\rm tmp} \approx \tau_{\rm r}$ (indicating very rapid variation of temperature), a proper overdamped description cannot be obtained, as explained in the Supplementary Note 5. Thus, in this study, we consider the following hierarchy of time scales to guarantee a proper overdamped limit: $\tau_{\rm r} \ll \tau_{\rm obs} \leq \tau_{\rm od} \approx \tau_{\rm tmp}$.

On these time scales, the systematic overdamped approximation can be carried out using Brinkman's hierarchy method[31,37]. This method provides a systematic way to expand the probability distribution $P_{\rm ud}$ and obtain the overdamped limit. Conventionally, there have been two approaches to such expansions: (i) the small-mass expansion and (ii) the inverse viscous (large γ) expansion. In the absence of time-varying temperature, these two expansions converge to the same overdamped limit with identical thermodynamics. However, in the presence of time-varying temperature, we find that the two expansions no longer converge to the same limiting thermodynamics. Mathematically, the limit $\tau \equiv \tau_{\rm od}/\tau_{\rm r} \gg 1$ alone is not sufficient to uniquely characterize the thermodynamics of the overdamped limit. In fact, apart from τ, another parameter, $\nu \equiv V_{\rm ud}/V_{\rm od}$, where $V_{\rm ud}$ and $V_{\rm od}$ represent the characteristic velocities in the underdamped and overdamped dynamics, respectively, plays a crucial role. (See Methods, near Eq. (21), for the definitions of $V_{\rm ud}$ and $V_{\rm od}$.) Essentially, the presence of time-dependent temperature turns this into a two-parameter expansion problem.

For mathematical convenience, we absorb the parameter ν into the dimensionless scaling exponent z via the relation $\nu = \tau^z$. This allows us to systematically investigate the overdamped behavior of the system for various values of z in the large-τ regime. As elaborated in the Methods section, we note that $z = 0$ corresponds to the inverse viscous expansion and therefore we call it the large-γ limit. Similarly, $z = 1/2$ corresponds to the small-mass expansion and therefore it is referred to as the small-m limit. Moreover, $0 < z < 1/2$ represents an intermediate overdamped regime, which has not been explored and may correspond to a specific overdamped experimental setup. Note that the overdamped limit formally exists for $\tau \gg 1$, where inertial effects become negligible compared to viscous damping. However, the precise thermodynamic behavior realized in this regime depends on the scaling parameter ν, which determines whether the system approaches the large-γ, the small-m limit, or an intermediate limit. In other words, while $\tau \gg 1$ ensures overdamped dynamics, the nature of the resulting limit is dictated by ν.

Through this method, we first derive the overdamped approximation of the underdamped FP equation (2). The detailed derivation is presented in the Methods section. Regardless of the z value, the resulting equation is the same as the usual overdamped FP equation, as shown below:

$$\partial_t P_{\rm od}(x, t) = -\partial_x J_{\rm od}(x, t), \tag{8}$$

where $P_{\rm od}(x, t) = \int dv P_{\rm ud}(x, v, t)$ and $J_{\rm od}(x, t) \equiv \gamma^{-1}\big(f(x, t) - T(t)\partial_x\big)P_{\rm od}(x, t)$. Therefore, the corresponding overdamped Langevin equation is

$$\gamma \dot{x}_t = f(x_t, \lambda_t) + \eta_t \,, \tag{9}$$

which is identical to the expression obtained by simply neglecting the inertia term in Eq. (1).

Thermodynamic anomalies

Conventionally, the mean heat rate of the overdamped equation (9) is known as[32]

$$\langle \dot{Q} \rangle_{\rm od} = -\langle f(x, \lambda) \circ \dot{x} \rangle_{\rm od} = -\int_{-\infty}^{\infty} dx f(x, \lambda) J_{\rm od}(x, t), \tag{10}$$

where $\langle \cdots \rangle_{\rm od}$ denotes the ensemble average taken over $P_{\rm od}(x, t)$. Additionally, the rate of total EP in the overdamped approximation is

conventionally expressed as[38,39]

$$\langle \dot{S}_{\rm tot}\rangle_{\rm od} = \int_{-\infty}^{\infty} dx\, \frac{\gamma J_{\rm od}^2}{T(t)P_{\rm od}}\,. \tag{11}$$

These two expressions, Eqs. (10) and (11), accurately quantify heat and EP in overdamped dynamics when the temperature is time-independent.

However, if the temperature has time dependence, the overdamped approximations of Eqs. (5) and (7) do not conincide with Eqs. (10) and (11), respectively. We refer to this discrepancy as the thermodynamic anomaly. Our main result is the explicit expressions for these anomalies. First, we calculate the heat anomaly, defined as $\mathscr{A}_Q \equiv \langle \dot{Q}\rangle_{\rm ud} - \langle \dot{Q}\rangle_{\rm od}$. To evaluate $\mathscr{A}_Q$, we need to expand $\langle \dot{Q}\rangle_{\rm ud}$ as a non-positive power series in τ. As explained in the Supplementary Note 2, the order of $\langle \dot{Q}\rangle_{\rm od}$ is $O(\tau^{-1+2z})$, which is less than or equal to the order of $\langle \dot{Q}\rangle_{\rm ud}$. Therefore, by retaining all terms up to order τ^{-1+2z} in the expansion, we can evaluate $\mathscr{A}_Q$ consistently up to the order of $\langle \dot{Q}\rangle_{\rm od}$. As detailed in the Supplementary Note 2, the result is

$$\mathscr{A}_Q = \begin{cases} \frac{\dot{T}}{2} - \frac{m\dddot{T}}{4\gamma} & \text{for } z = 0\,, \\ \frac{\dot{T}}{2} & \text{for } 0 < z \le 1/2\,. \end{cases} \tag{12}$$

Therefore, the anomaly depends on z, unlike the dynamic equation. The orders of the terms $\dot{T}/2$ and $m\ddot{T}/4\gamma$ are $O(\tau^0)$ and $O(\tau^{-1})$, respectively, and are independent of z. In contrast, the order of $\langle \dot{Q}\rangle_{\rm od}$ depends on z and is given by $O(\tau^{-1+2z})$. Therefore, for $z = 0$ (high-viscosity regime), among the three terms contributing to $\langle \dot{Q}\rangle_{\rm ud}$, $\dot{T}/2$ is the leading-order term, while the other two terms, $\langle \dot{Q}\rangle_{\rm od}$ and $m\ddot{T}/4\gamma$, are of the same higher order $O(\tau^{-1})$. For $0 < z < 1/2$, $\langle \dot{Q}\rangle_{\rm od}$ is of higher order than $\dot{T}/2$. Finally, for $z = 1/2$ (small-mass regime), $\dot{T}/2$ and $\langle \dot{Q}\rangle_{\rm od}$ are of the same order, $O(\tau^0)$. Note that the order of each term mentioned above is estimated using the dimensionless formalism presented in the Methods section. An interesting feature of $\mathscr{A}_Q$ is that the time-accumulated $\mathscr{A}_Q$ depends only on the initial and final information of the temperature, not on the temporal protocol, even though heat is not a state variable. Furthermore, $\mathscr{A}_Q$ is independent of the external force applied to the system.

The heat anomaly arises from neglecting the velocity degree of freedom in the overdamped approximation. This approximation implicitly assumes that the velocity is always relaxed to its equilibrium state. Consequently, for constant temperature, the kinetic energy $E_{\rm K}$ remains unchanged, resulting in no additional heat exchange with the environment. However, when the temperature varies with time, $E_{\rm K}$ also changes, leading to additional heat exchange with the environment. This is the origin of the heat anomaly. As demonstrated in Supplementary Note 4, an explicit relation between $\mathscr{A}_Q$ and $E_{\rm K}$ is given by

$$\langle \dot{E}_{\rm K}\rangle = \mathscr{A}_Q \text{ or } \langle E_{\rm K}\rangle_{\rm ud} = \begin{cases} \frac{T}{2} - \frac{m\dot{T}}{4\gamma} & \text{for } z = 0\,, \\ \frac{T}{2} & \text{for } 0 < z \le 1/2\,. \end{cases} \tag{13}$$

up to the order of $\langle \dot{Q}\rangle_{\rm od}$.

Similarly to the case of heat, the total EP exhibits a discrepancy between Eq. (7) and Eq. (11). The EP anomaly, defined as $\mathscr{A}_S \equiv \langle \dot{S}_{\rm tot}\rangle_{\rm ud} - \langle \dot{S}_{\rm tot}\rangle_{\rm od}$ up to the same order of $\langle \dot{S}_{\rm tot}\rangle_{\rm od}$, is

$$\mathscr{A}_S = \begin{cases} \frac{m}{4\gamma}\left(\frac{\dot{T}}{T}\right)^2 & \text{if } z = 0\,, \\ 0 & \text{if } 0 < z \le 1/2\,. \end{cases} \tag{14}$$

The details of the calculations are provided in Supplementary Note 3. Thus, $\mathscr{A}_S$ also depends on z. The order of $\frac{m}{4\gamma}(\dot{T}/T)^2$ is $O(\tau^{-1})$ and is independent of z, whereas the order of $\langle \dot{S}_{\rm tot}\rangle_{\rm od}$ is $O(\tau^{-1+2z})$. Therefore, for $z = 0$, the orders of $\langle \dot{S}_{\rm tot}\rangle_{\rm od}$ and $\frac{m}{4\gamma}(\dot{T}/T)^2$ are the same, $O(\tau^{-1})$. For $0 < z \le 1/2$, there is no EP anomaly appears in this range of z, even though $\mathscr{A}_Q$ remains finite. Unlike $\mathscr{A}_Q$, the time-accumulated $\mathscr{A}_S$ for $z = 0$ depends on the temporal protocol of the temperature due to the squared term of the time derivative of the temperature. Moreover, Eq. (14) indicates that $\langle \dot{S}_{\rm tot}\rangle_{\rm ud} \ge \langle \dot{S}_{\rm tot}\rangle_{\rm od}$. Similar to the case of position-dependent temperature[11], the finite $\mathscr{A}_S$ for $z = 0$ originates from the breaking of time- and velocity-reversal symmetry at the microscopic level. However, for $0 < z \le 1/2$, the extent of this symmetry breaking is negligible compared to $\langle \dot{S}_{\rm tot}\rangle_{\rm od}$, leading to the absence of the anomaly.

Estimation and control of z

In general, a system becomes overdamped for large τ. However, the specific nature of the overdamped system is determined by the parameter z; in particular, the thermodynamic anomalies depend on z. Thus, identifying or controlling z of a given system is crucial for precisely estimating the anomalies in overdamped dynamics. Yet, it is not straightforward to estimate z directly from experimental or simulation setups. Therefore, it is necessary to devise a scheme for its estimation.

Here, we propose an experimental or simulation method to estimate or control the exponent z. Adjusting z can be achieved by simultaneously varying the amplitudes of both the external force and the temperature. The underlying framework used in our analysis is the Brinkmann hierarchy, which is constructed by expanding the probability density in Hermite polynomials of the velocity variable. This expansion transforms the Fokker-Planck equation of the underdamped dynamics into an infinite hierarchy of coupled equations for the expansion coefficients, (see Methods, Eqs. (18)-(20)), thereby systematically capturing the dynamics across progressively higher moments. This coupled coefficient equation can be recast in dimensionless form, Eq. (21), by introducing dimensionless time, position, and temperature. This dimensionless equation is necessary for performing a systematic expansion in terms of the dimensionless parameter τ. To illustrate the estimation scheme for z, we consider how the following magnitude adjustments of the force and temperature affect the dimensionless coupled hierarchy equations:

$$f \to \tau^{-\zeta} f \quad \text{and} \quad T \to \tau^{-\zeta} T, \tag{15}$$

where ζ serves as a control parameter. Under this transformation, the dimensionless equation (21) remains invariant, with the only modification being a shift from $\nu = \tau^z$ to $\nu' \equiv \tau^{z-\zeta/2}$ as shown in Eq. (22). The details of the transformation are provided in the Methods section. This clearly indicates that the exponent z can be controlled by adjusting ζ, or equivalently, by varying the magnitudes of f and T.

In practice, the exponent can be estimated or set to an appropriate value by comparing the magnitudes of the $\dot{T}/2$, $\langle \dot{Q}\rangle_{\rm od}$, and $m\ddot{T}/(4\gamma)$. In the setup with the magnitude adjustment (15), the orders of $\dot{T}/2$ and $m\ddot{T}/(4\gamma)$ are $O(\tau^0)$ and $O(\tau^{-1})$, respectively, whereas the order of $\langle \dot{Q}\rangle_{\rm od}$ depends on $z - \zeta/2$ as $\langle \dot{Q}\rangle_{\rm od} \sim O(\tau^{-1+2(z-\zeta/2)})$. Now, we can estimate $\dot{T}/2$, $\langle \dot{Q}\rangle_{\rm od}$, and $m\ddot{T}/(4\gamma)$ by varying ζ, as shown in Fig. 1. If the magnitudes of $\langle \dot{Q}\rangle_{\rm od}$ and $m\ddot{T}/(4\gamma)$ become comparable, it implies that $-1 + 2(z - \zeta/2) \approx -1$, which yields $z \approx \zeta/2$. On the other hand, if the magnitudes of $\langle \dot{Q}\rangle_{\rm od}$ and $\dot{T}/2$ become comparable, it signifies $-1 + 2(z - \zeta/2) \approx 0$, which yields $z \approx \zeta/2 + 1/2$.

To verify this method numerically, we consider a Langevin system with an external force $f = k_0 x$ and a time-dependent temperature $T(t) = 2 + \sin(t)$. Here, we set $\tau_{\rm tmp} = 2\pi = \tau_{\rm od}$, which is the period of the temperature variation. Thus, $\tau = 2\pi\gamma/m$. The parameters are set as $k_0 = 1$, $\gamma = 1$, and $m = 0.01$ (small-m condition). Figure 1 shows the plots of $\langle \dot{Q}\rangle_{\rm od}$, $\dot{T}/2$, and $m\ddot{T}/(4\gamma)$ as functions of ζ. Comparing the magnitudes of $\langle \dot{Q}\rangle_{\rm od}$ with $m\ddot{T}/(4\gamma)$ or $\dot{T}/2$ consistently leads to $z \approx 1/2$, which corresponds to the small-m setup.

The emergence of the value $z = 1/2$ can also be understood as follows. The relation $v = \tau^z = V_{ud}/V_{od}$ leads to

$$z = \frac{\ln \frac{V_{ud}}{V_{od}}}{\ln \frac{\tau_{od}}{\tau_r}} = \frac{\ln\left(\sqrt{\frac{T_0}{m}}\frac{\tau_{od}}{l_{od}}\right)}{\ln\left(\frac{\tau_{od}\gamma}{m}\right)}, \tag{16}$$

where the expressions for V_{ud} and V_{od} are given in Eq. (21). The typical length scale of this systems l_{od} can be defined from the second moment of the distribution, i.e., $l_{od} \sim \sqrt{\langle x^2 \rangle} \sim \sqrt{T_0/k_0}$. Then, Eq. (16) reduces to

$$z = \frac{\ln \tau_{od} - \frac{1}{2}\ln m}{\ln \tau_{od} - \ln m}, \tag{17}$$

where $k_0 = 1$ and $\gamma = 1$ are used. Here, τ_{od} can be chosen as either $\gamma/k_0 = 1$ or $\tau_{tmp} = 2\pi$. However, regardless of the choice of τ_{od}, z approaches 1/2 in the small-m limit.

We note that the exponent can also be extracted from the scaling behavior of $\langle \dot{Q} \rangle_{od} \sim \tau^{-1+2z}$ by varying τ. However, this approach may not be suitable, as adjusting τ requires varying m or γ, which are typically fixed parameters in most experimental setups rather than controllable variables. In contrast, adjusting the magnitudes of f and T is more straightforward.

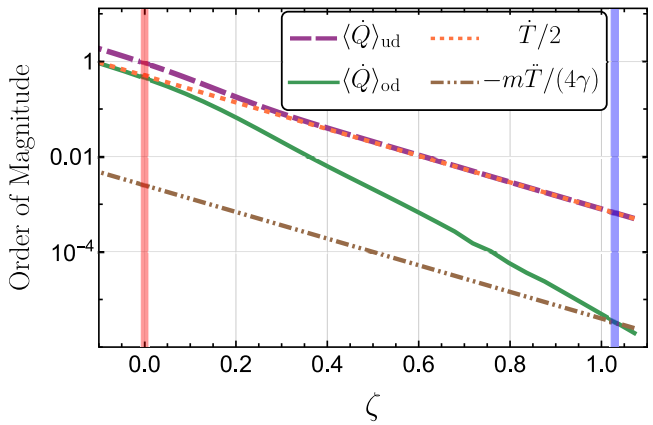

Fig. 1 | Control parameter dependence of heat-rate and anomaly magnitudes. Order-of-magnitude plot of the underdamped heat rate $\langle \dot{Q} \rangle_{ud}$, overdamped heat rate $\langle \dot{Q} \rangle_{od}$, and the two heat anomaly terms $\dot{T}/2$ and $m\ddot{T}/(4\gamma)$ as functions of the control parameter ζ for a particle confined in a harmonic trap and immersed in bath with time-periodic temperature $T(t) = 2 + \sin(t)$. The parameters used for this plot are stiffness $k_0 = 1$, viscous coefficient $\gamma = 1$, and mass $m = 0.01$. The ζ values at the two crossing points - between $\langle \dot{Q} \rangle_{od}$ and $\dot{T}/2$, and between $\langle \dot{Q} \rangle_{od}$ and $m\ddot{T}/(4\gamma)$ - are highlighted by the orange and purple vertical lines, respectively. The orange and purple lines are located at $\zeta \approx 0$ and $\zeta \approx 1.03$, respectively. These crossing points are used to estimate the exponent z, which is found to be $z \approx 1/2$. For each ζ, the values of $\langle \dot{Q} \rangle_{ud}$, $\langle \dot{Q} \rangle_{od}$, $\dot{T}/2$, and $m\ddot{T}/(4\gamma)$ correspond to their maximum absolute values within one period in the periodic steady state.

To validate our theoretical results numerically, we simulate the engine model for three different values of γ, while keeping all other parameters fixed. Figure 3 shows the plots of the three heat rates, $\langle \dot{Q} \rangle_{ud}$, $\langle \dot{Q} \rangle_{od}$, and $\langle \dot{Q} \rangle_{od+an} = \langle \dot{Q} \rangle_{od} + \mathscr{A}_Q$, as functions of time for $\gamma = 10$, 100, and 1000. In this calculation, $\mathscr{A}_Q$ for $z = 0$ is used, since the mass is taken to be of order unity in this example. As shown in the figure, for $\gamma = 10$, the three heat rates do not coincide, because γ is not sufficiently large to ensure the validity of the overdamped approximation. However, as γ increases, $\langle \dot{Q} \rangle_{od+an}$ approaches $\langle \dot{Q} \rangle_{ud}$, whereas $\langle \dot{Q} \rangle_{od}$ does not. $\langle \dot{Q} \rangle_{od}$ coincides with $\langle \dot{Q} \rangle_{ud}$ only during the isothermal process, where the temperature remains constant and no heat anomaly arises. We note that constructing finite-time adiabatic processes in the underdamped regime remains an open challenge[40]. Therefore, we adopt an adiabatic process in which heat does not flow only in the quasi-static limit[41].

Heat rate in heat engine

The effects of the thermodynamic anomalies can be significant in engine systems. As an example, consider a Brownian Carnot engine experimentally realized by Martínez et al.[6]. The schematic diagram of the engine is depicted in Fig. 2(a). In this engine, a Brownian particle is confined in harmonic potential with a time-dependent stiffness $k(t)$: during the compression phase $0 \le t < t_p/2$, $k(t) = k_0 + k_1 t^2/t_p^2$; during the expansion phase $t_p/2 \le t < t_p$, $k(t) = k_0 + k_1(t_p - t)^2/t_p^2$, where t_p denotes the period of the engine. Each cycle of the engine is divided into four processes based on the temperature variation: (i) an isothermal process, $T(t) = T_c$ for $0 \le t < t_p/4$; (ii) an adiabatic process, $T(t) = T_c\sqrt{k(t)/k(t_p/4)}$ for $t_p/4 \le t < t_p/2$; (iii) an isothermal process, $T(t) = T_h$ for $t_p/2 \le t < 3t_p/4$; and (iv) an adiabatic process, $T(t) = T_h\sqrt{k(t)/k(3t_p/4)}$ for $3t_p/4 \le t < t_p$. The time variations of $k(t)$ and $T(t)$ are visually presented in Supplementary Note 6.

Efficiency of heat engine

Under the same setup, we evaluate the three different efficiencies: η_{ud}, η_{od}, and η_{ud+an} using the underdamped formulation, overdamped formulation, and overdamped formulation incorporating the heat anomaly, respectively. To operate the engine close to the quasi-static limit, we increase t_p to 50, 000. The details are presented in the Methods section. Figure 3(b) shows the resulting plots of η_{ud}, η_{od}, and η_{od+an} as functions of γ. Here, $\mathscr{A}_Q$ for $z = 0$ is used to evaluate η_{od+an}. Note that the contribution of the anomaly to heat becomes more significant in the large-γ regime, as presented in Supplementary Note 2. This results in the efficiency discrepancy between η_{od} and η_{od+an}. As γ increases, only η_{od+an} converges to η_{ud}, whereas η_{od} deviates significantly from the other two. This highlights the substantial impact of the anomalies on the accurate calculation of thermodynamic quantities in heat engines.

Estimation of kinetic energy

In some cases, evaluating kinetic energy in overdamped systems is necessary for accurately estimating thermodynamic quantities[6,42]. However, directly

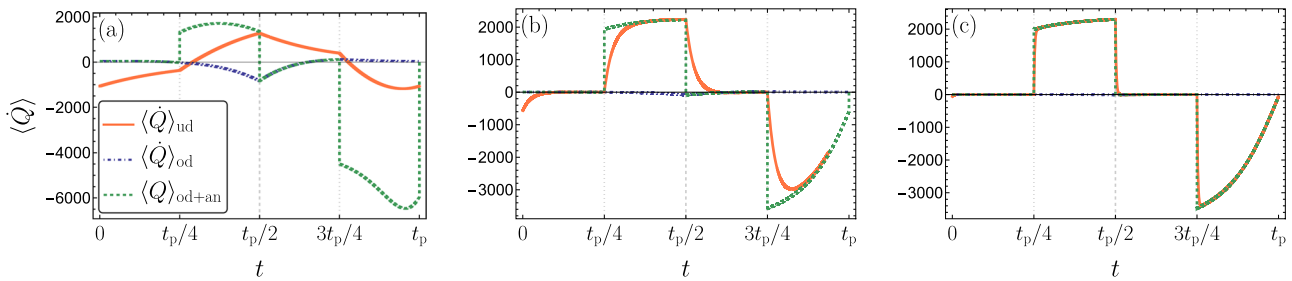

Fig. 2 | Heat-rate evolution for overdamped, underdamped, and anomaly-adjusted dynamics. Mean heat rate as a function of time t for the overdamped case $\langle \dot{Q} \rangle_{od}$, underdamped case $\langle \dot{Q} \rangle_{ud}$ and anomaly adjusted overdamped case $\langle \dot{Q} \rangle_{ud+an}$. Parameters: time period $t_p = 0.2$, mass $m = 1$, and viscosity coefficient (**a**) $\gamma = 10$, (**b**) $\gamma = 100$, (**c**) $\gamma = 1000$.

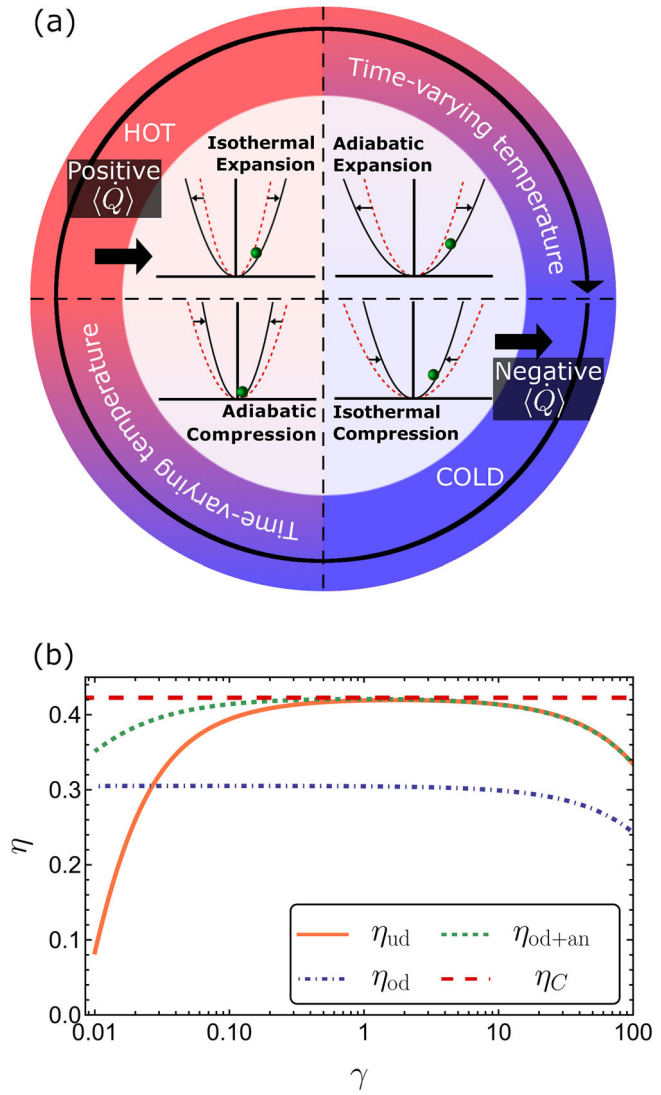

Fig. 3 | Numerical analysis of a finite-time Brownian Carnot engine. a Schematic diagram of a Brownian Carnot Engine depicting its four stages of operation in each time-cycle. The figure shows the thermodynamic cycle of the engine in a clockwise direction, consisting of four key processes: isothermal compression, adiabatic compression, isothermal expansion, and adiabatic expansion. The temperature of the surrounding heat bath is represented by the outer colored ring, while the compression and expansion processes are indicated by variations in potential strength within each quadrant. **b** Efficiencies $\eta_{\rm ud}$, $\eta_{\rm od}$, and $\eta_{\rm od+an}$ as a function of γ for the Brownian Carnot engine. The Carnot efficiency bound η_C is also shown in the plot for reference.

measuring kinetic energy in such systems is experimentally challenging, as velocity rapidly relaxes to equilibrium. Therefore, state-of-the-art experimental setups[43–45] are required for precise kinetic energy measurements. To overcome this technical difficulty, a method, called time-averaged velocity (TAV) method, for estimating kinetic energy was proposed, where kinetic energy is inferred from measurements of the mean square velocity sampled at frequencies several orders of magnitude lower than the velocity relaxation frequency[42]. However, the TAV method, is limited to systems with a Brownian particle trapped in a harmonic potential and is accurate only for quasi-static processes, failing for moderately fast temperature variations, as shown in Supplementary Note 7. In contrast, Eq. (13) directly provides an accurate kinetic energy estimate even for rapidly varying temperatures. Performance comparisons between the TAV method and our approach are presented in Supplementary Note 7.

Discussion

We derive explicit expressions for heat and EP anomalies in systems immersed in an environment with a general time-varying temperature. Using a cyclic engine as an example, we demonstrate that thermodynamic quantities such as heat and efficiency estimated within the overdamped description can significantly deviate from their correct values if these anomalies are not properly considered. An important point is that these anomalies depend on the exponent z, which relates the two scaling parameters, ν and τ, introduced for the systematic overdamped approximation. Therefore, it is crucial to estimate z for precise calculation of thermodynamic quantities. We propose an experimental method to estimate or control z by adjusting the amplitudes of force and temperature. It is worth noting that the applicability of our method extends beyond the linear regime developed by Brandner et al.[46], where the variations in temperature and force are small.

Our results allow for accurate estimation of thermodynamic quantities in overdamped systems without requiring complex or challenging experimental techniques to directly measure the system's fast-relaxing velocity. Instead, by simply incorporating the anomalies into the corresponding quantities computed within the overdamped description, we can achieve accurate measurements. Furthermore, our findings provide a straightforward method for estimating kinetic energy even for overdamped systems. Consequently, our results offer the systematic way for an accurate study of thermodynamics in a wide range of overdamped systems with time-varying temperature. One particularly interesting example is an overdamped particle subject to active Ornstein-Uhlenbeck process (AOUP) noise[47]. This system can be mapped onto an effective underdamped dynamics, from which the overdamped dynamics can be derived in the small-persistence-time limit. Since this mathematical setup is essentially the same as ours, we expect that our method can serve as a platform for evaluating accurate thermodynamic quantities in active systems.

Since our analysis is based on the condition that the temperature variation is not rapid ($\tau_{\rm tmp} \approx \tau_{\rm od}$), it is worth commenting on the relevance and limitations of applying our anomaly estimates to quenching protocols, where the bath temperature changes instantaneously. For example, recent studies[48,49] have demonstrated that instantaneous temperature variation can be used to make an optimal protocol for connecting distinct states. As noted in the Supplementary Note 5, a rigorous overdamped limit cannot be achieved when the temperature varies rapidly ($\tau_{\rm tmp} \approx \tau_{\rm r}$). In such cases, the dynamics should, in principle, be described by underdamped equations. Thus, investigation of anomalies under rapidly varying temperature protocols is left for future work. Nevertheless, apart from the very short duration of rapid temperature changes, our overdamped formalism remains applicable in a piecewise manner.

Methods

Brinkman's hierarchy method with two scaling parameters

Define $\bar{P}_{\rm ud} \equiv \psi_0^{-1} P_{\rm ud}(x, v, t)$, where $\psi_0 = Ne^{-\Phi/2}$ with the normalization factor $N \equiv \left[2\pi T(t)/m\right]^{-1/4}$ and $\Phi \equiv \frac{mv^2}{2T(t)}$. Using the nth eigenfunction ψ_n of a harmonic oscillator given by

$$\psi_n = \frac{1}{\sqrt{2^n n!}} \psi_0 H_n\left(\sqrt{\frac{m}{2T(t)}} v\right), \tag{18}$$

where $H_n(x)$ denotes the Hermite polynomial, $\bar{P}_{\rm ud}$ can be expanded as

$$\bar{P}_{\rm ud} = \sum_{n=0}^{\infty} c_n(x, t)\psi_n . \tag{19}$$

Note that $c_0(x, t) = P_{\rm od}(x, t)$ as explained in Supplementary Note 1. Substituting Eq. (19) into the Hermitianized Fokker-Planck equation yields the

following coupled equation for the coefficients c_n (for $n \geq 0$):

$$\partial_t c_n = -\sqrt{\frac{(n+1)T(t)}{m}}\partial_x c_{n+1} + \frac{\sqrt{n}}{\sqrt{mT(t)}}\left[f(x,\lambda_t) - T(t)\partial_x\right]c_{n-1} - \frac{n\gamma}{m}c_n - \frac{\dot{T}(t)}{2T(t)}\left(\sqrt{n(n-1)}c_{n-2} + nc_n\right). \tag{20}$$

The detailed derivation of Eq. (20) is provided in Supplementary Note 1.

Furthermore, it is shown in SM that the high-viscosity and the small-mass limits result in different expressions for heat and EP. To address this in a systematic way, here, we present a unified perturbative scheme, Brinkman's hierarchy with two-scaling parameters, capable of exploring not only these two limits but also the intermediate regimes.

To achieve this, we convert Eq. (20) into a dimensionless form by introducing the characteristic time and length scales of the overdamped system, denoted as $\tau_{\rm od}$ and $l_{\rm od}$, respectively. We note that although there is freedom in choosing the specific value of $\tau_{\rm od}$, the choice is not arbitrary, as our analysis is carried out under the condition $\tau_{\rm od} \approx \tau_{\rm tmp}$. Using these, we define the dimensionless time, position, and nth coefficient as $\bar{t} \equiv t/\tau_{\rm od}$, $\bar{x} \equiv x/l_{\rm od}$, and $\bar{c}_n \equiv l_{\rm od}c_n$, respectively. Additionally, we introduce a dimensionless temperature $\bar{T}(t) \equiv T(t)/T_0$, where T_0 represents the typical energy scale of the system. These definitions allow us to specify the typical velocities of the underdamped system, $V_{\rm ud} \equiv \sqrt{T_0/m}$, and the overdamped system, $V_{\rm od} \equiv l_{\rm od}/\tau_{\rm od}$. Using the quantities defined thus far, we can rewrite Eq. (20) in a dimensionless form as follows:

$$\partial_{\bar{t}}\bar{c}_n = -\nu\sqrt{(n+1)\bar{T}(t)}\partial_{\bar{x}}\bar{c}_{n+1} + \nu\sqrt{n\bar{T}(t)}\left[\frac{\bar{f}(x,\lambda_t)}{\bar{T}(t)} - \partial_{\bar{x}}\right]\bar{c}_{n-1} - \tau n\bar{c}_n - \frac{\dot{\bar{T}}(t)}{2\bar{T}(t)}\left(\sqrt{n(n-1)}\bar{c}_{n-2} + n\bar{c}_n\right), \tag{21}$$

where $\nu \equiv V_{\rm ud}/V_{\rm od}$, $\tau \equiv \tau_{\rm od}/\tau_{\rm r}$, $\dot{\bar{T}} = d\bar{T}/d\bar{t}$, and $\bar{f} \equiv (l_{\rm od}/T_0)f$ is the dimensionless force.

Instead of the two parameters m and γ in Eq. (20), whose magnitudes govern the overdamped approximation, the two dimensionless parameters τ and ν in Eq. (21) now play this role. Here, τ is large ($\tau \gg 1$) because we focus on the time scales $\tau_{\rm r} \ll \tau_{\rm obs} \leq \tau_{\rm od} \approx \tau_{\rm tmp}$. We also anticipate $\nu \gg 1$, as $V_{\rm ud} \gg V_{\rm od}$ is typically expected. To systematically expand the orders in Eq. (21), we need to establish the magnitude relationship between τ and ν. For simplicity, we set $\nu = \tau^z$, where $z \geq 0$, indicating that ν is of order $O(\tau^z)$. We note that $z = 0$ leads to $m \sim T_0\tau_{\rm od}^2/l_{\rm od}^2$. Thus, m is a $O(1)$ quantity in the dimensionless form, which implies that γ must be large to satisfy the condition $\tau \gg 1$. Therefore, $z = 0$ corresponds to the high-viscosity limit. On the other hand, $z = 1/2$ gives $\gamma \sim T_0\tau_{\rm od}/l_{\rm od}^2$. In this case, γ is a $O(1)$ quantity in the dimensionless equation, which implies that m must be small. Therefore, $z = 1/2$ corresponds to the small-mass limit. Finally, $0 < z < 1/2$ represents an intermediate regime between the high-viscosity and small-mass limits.

Note that the force and temperature transformations specified in Eq. (15) lead to

$$\partial_{\bar{t}}\bar{c}_n = -\tau^{z-\frac{\zeta}{2}}\sqrt{(n+1)\bar{T}(t)}\partial_{\bar{x}}\bar{c}_{n+1} + \tau^{z-\frac{\zeta}{2}}\sqrt{n\bar{T}(t)}\left[\frac{\bar{f}(x,\lambda_t)}{\bar{T}(t)} - \partial_{\bar{x}}\right]\bar{c}_{n-1} - \tau n\bar{c}_n - \frac{\dot{\bar{T}}(t)}{2\bar{T}(t)}\left(\sqrt{n(n-1)}\bar{c}_{n-2} + n\bar{c}_n\right). \tag{22}$$

Thus, the transformation does not alter the functional form of Eq. (21) except for the rescaling of the dimensionless parameter from $\nu = \tau^z$ to $\nu' \equiv \tau^{z-\zeta/2}$. This exponent shift by $\zeta/2$ arises directly from the combined scaling of the force amplitude and the temperature. The rescaling fully captures the impact of the transformation on the dynamical behavior encoded by Eq. (21). Therefore, this transformation can be used to control the parameter ν for the overdamped approximation.

For $0 \leq z \leq 1/2$, substituting $\nu = \tau^z$ into Eq. (21) and collecting the leading-order terms result in (for $n = 0, 1$),

$$\partial_{\bar{t}}\bar{c}_0 = -\tau^z\sqrt{\bar{T}}\partial_{\bar{x}}\bar{c}_1\,, \tag{23}$$

$$\bar{c}_1 = \tau^{z-1}\sqrt{\bar{T}(t)}\left(\bar{f}/\bar{T} - \partial_{\bar{x}}\right)\bar{c}_0\,. \tag{24}$$

Plugging Eq. (24) into Eq. (23) leads to the following dimensionless FP equation:

$$\partial_{\bar{t}}\bar{c}_0 = -\partial_{\bar{x}}\bar{J}(x,t)\,. \tag{25}$$

where the dimensionless probability current $\bar{J}(x,t)$ is given by

$$\bar{J}(x,t) = \tau^{2z-1}\left(\bar{f} - \bar{T}\partial_{\bar{x}}\right)\bar{c}_0\,. \tag{26}$$

As $\bar{J}(x,t)$ diverges for $z > 1/2$, which is physically infeasible, we restrict our attention to the regime $0 \leq z \leq 1/2$. Note that if we convert the dimensionless variables in Eq. (25) back to their original forms, the equation becomes identical to Eq. (8). This shows that the dynamic equations for overdamped systems are independent of z.

Three different efficiencies: $\eta_{\rm ud}$, $\eta_{\rm od}$, and $\eta_{\rm od+an}$

Under the setup described in the "Efficiency of heat engine" section, we numerically evaluate the engine efficiency $\eta = \langle W\rangle / \langle Q_{\rm in}\rangle$ in a periodic steady state, where $\langle W\rangle = \int_{t=0}^{t_{\rm p}} d\dot{t}k\langle x^2\rangle/2$ represents work done by the engine and $\langle Q_{\rm in}\rangle = \int_0^{t_{\rm p}} dt\Theta(\langle\dot{Q}\rangle)\langle\dot{Q}\rangle$ denotes the heat input to the engine. Here, the Heaviside function $\Theta(x)$ is defined as $\Theta(x) = 1$ for $x > 0$ and $\Theta(x) = 0$ otherwise. For this calculation, the parameters are set as $k_0 = 2$, $k_1 = 64$, $T_c = 300$, $T_h = T_c\sqrt{k(t_{\rm p}/2)/k(t_{\rm p}/4)}$, $t_{\rm p} = 10^3$, and $m = 1$. We evaluate the input heat in three different ways: using the underdamped formulation (4), $\langle Q_{\rm in}\rangle_{\rm ud} = \int_0^{t_{\rm p}} dt\Theta(\langle\dot{Q}\rangle_{\rm ud})\langle\dot{Q}\rangle_{\rm ud}$; using the overdamped formulation (10), $\langle Q_{\rm in}\rangle_{\rm od} = \int_0^{t_{\rm p}} dt\Theta(\langle\dot{Q}\rangle_{\rm od})\langle\dot{Q}\rangle_{\rm od}$; and using the overdamped formulation with the addition of the heat anomaly (12), $\langle Q_{\rm in}\rangle_{\rm od+an} = \int_0^{t_{\rm p}} dt\Theta(\langle\dot{Q}\rangle_{\rm od} + \mathscr{A}_Q)(\langle\dot{Q}\rangle_{\rm od} + \mathscr{A}_Q)$. This definition of heat input, based on the Heaviside function, has been frequently used despite its drawbacks[47]. We can also use the alternative definition of heat input, such as that suggested by Giulia Gronchi and Andrea Puglisi[47] (see Eq. (6) of the reference). As a concrete example, we recalculated the efficiency using this alternative definition and presented the result in Fig. S2 of the Supplementary Note 6.

Note that $\langle W\rangle$ does not depend on whether the underlying dynamics are underdamped or overdamped, as the work is evaluated solely using position trajectories. Then, the efficiency can also be defined in three ways: $\eta_{\rm ud} \equiv \langle W\rangle/\langle Q_{\rm in}\rangle_{\rm ud}$, $\eta_{\rm od} \equiv \langle W\rangle/\langle Q_{\rm in}\rangle_{\rm od}$, and $\eta_{\rm od+an} \equiv \langle W\rangle/\langle Q_{\rm in}\rangle_{\rm od+an}$.

Data availability

Detailed analytical derivations and numerical estimates are provided in the Supplementary Information (SI) document. The numerical source data underlying the plots are provided in the Supplementary Data file. Additional data supporting the findings of this study are available from the corresponding author upon request.

Code availability

Source code is available from the corresponding authors upon request.

Received: 7 April 2025; Accepted: 18 February 2026;
Published online: 09 March 2026

References

1. Whalen, S., Thompson, M., Bahr, D., Richards, C. & Richards, R. Design, fabrication and testing of the p3 micro heat engine. *Sens. Actuators A: Phys.* **104**, 290 (2003).
2. Blickle, V. & Bechinger, C. Realization of a micrometre-sized stochastic heat engine. *Nat. Phys.* **8**, 143 (2012).
3. Steeneken, P. et al. Piezoresistive heat engine and refrigerator. *Nat. Phys.* **7**, 354 (2011).
4. Brantut, J.-P. et al. A thermoelectric heat engine with ultracold atoms. *Science* **342**, 713 (2013).
5. Argun, A. et al. Experimental realization of a minimal microscopic heat engine. *Phys. Rev. E* **96**, 052106 (2017).
6. Martínez, I. A. et al. Brownian carnot engine. *Nat. Phys.* **12**, 67 (2016).
7. Krishnamurthy, S., Ghosh, S., Chatterji, D., Ganapathy, R. & Sood, A. A micrometre-sized heat engine operating between bacterial reservoirs. *Nat. Phys.* **12**, 1134 (2016).
8. Krishnamurthy, S., Ganapathy, R. & Sood, A. Overcoming power-efficiency tradeoff in a micro heat engine by engineered system-bath interactions. *Nat. Commun.* **14**, 6842 (2023).
9. Widder, M. & Titulaer, U. Brownian motion in a medium with inhomogeneous temperature. *Phys. A: Stat. Mech. its Appl.* **154**, 452 (1989).
10. Hondou, T. & Sekimoto, K. Unattainability of carnot efficiency in the brownian heat engine. *Phys. Rev. E* **62**, 6021 (2000).
11. Celani, A., Bo, S., Eichhorn, R. & Aurell, E. Anomalous thermodynamics at the microscale. *Phys. Rev. Lett.* **109**, 260603 (2012).
12. Bo, S., Aurell, E., Eichhorn, R. & Celani, A. Optimal stochastic transport in inhomogeneous thermal environments. *Europhys. Lett.* **103**, 10010 (2013).
13. Kawaguchi, K. & Nakayama, Y. Fluctuation theorem for hidden entropy production. *Phys. Rev. E* **88**, 022147 (2013).
14. Polettini, M. Diffusion in nonuniform temperature and its geometric analog. *Phys. Rev. E - Stat. Nonlinear Soft Matter Phys.* **87**, 032126 (2013).
15. Sancho, J. Brownian colloids in underdamped and overdamped regimes with nonhomogeneous temperature. *Phys. Rev. E* **92**, 062110 (2015).
16. Marino, R., Eichhorn, R. & Aurell, E. Entropy production of a brownian ellipsoid in the overdamped limit. *Phys. Rev. E* **93**, 012132 (2016).
17. Schmiedl, T. & Seifert, U. Efficiency at maximum power: an analytically solvable model for stochastic heat engines. *Europhys. Lett.* **81**, 20003 (2007).
18. Arold, D., Dechant, A. & Lutz, E. Heat leakage in overdamped harmonic systems. *Phys. Rev. E* **97**, 022131 (2018).
19. Awasthi, S. & Dutta, S. B. Oscillating states of driven Langevin systems under large viscous drives. *Phys. Rev. E* **106**, 064116 (2022).
20. Parrondo, J. M. & Espa nol, P. Criticism of Feynman's analysis of the ratchet as an engine. *Am. J. Phys.* **64**, 1125 (1996).
21. Derényi, I. & Astumian, R. D. Efficiency of brownian heat engines. *Phys. Rev. E* **59**, R6219 (1999).
22. Van den Broeck, C. Thermodynamic efficiency at maximum power. *Phys. Rev. Lett.* **95**, 190602 (2005).
23. Rana, S., Pal, P., Saha, A. & Jayannavar, A. Single-particle stochastic heat engine. *Phys. Rev. E* **90**, 042146 (2014).
24. Park, J.-M., Lee, J. S. & Noh, J. D. Optimal tuning of a confined Brownian information engine. *Phys. Rev. E* **93**, 032146 (2016).
25. Roßnagel, J. et al. A single-atom heat engine. *Science* **352**, 325 (2016).
26. Martínez, I. A., Roldán, É, Dinis, L. & Rica, R. A. Colloidal heat engines: a review. *Soft matter* **13**, 22–36 (2017).
27. Lee, J. S., Park, J.-M. & Park, H. Thermodynamic uncertainty relation for underdamped Langevin systems driven by a velocity-dependent force. *Phys. Rev. E* **100**, 062132 (2019).
28. Holubec, V. & Marathe, R. Underdamped active brownian heat engine. *Phys. Rev. E* **102**, 060101 (2020).
29. Chen, L., Qi, C., Ge, Y. & Feng, H. Thermal brownian heat engine with external and internal irreversibilities. *Energy* **255**, 124582 (2022).
30. Majumdar, R., Saha, A. & Marathe, R. Exactly solvable model of a passive brownian heat engine and its comparison with active engines. *J. Stat. Mech. Theory Exp.* **2022**, 073206 (2022).
31. Risken, H. The Fokker–Planck Equation: Methods of Solution and Applications, 2nd edn (Springer-Verlag Berlin Heidelberg, 1996).
32. Sekimoto, K. Langevin equation and thermodynamics. *Prog. Theor. Phys. Suppl.* **130**, 17 (1998).
33. Lee, S. et al. Multidimensional entropic bound: Estimator of entropy production for Langevin dynamics with an arbitrary time-dependent protocol. *Phys. Rev. Res.* **5**, 013194 (2023).
34. Dechant, A. & Sasa, S. -i Entropic bounds on currents in langevin systems. *Phys. Rev. E* **97**, 062101 (2018).
35. Spinney, R. E. & Ford, I. J. Entropy production in full phase space for continuous stochastic dynamics. *Phys. Rev. E* **85**, 051113 (2012).
36. Kwon, E., Park, J.-M., Lee, J. S. & Baek, Y. Unified hierarchical relationship between thermodynamic tradeoff relations. *Phys. Rev. E* **110**, 044131 (2024).
37. Brinkman, H. Brownian motion in a field of force and the diffusion theory of chemical reactions. *Physica* **22**, 29 (1956).
38. Seifert, U. Entropy production along a stochastic trajectory and an integral fluctuation theorem. *Phys. Rev. Lett.* **95**, 040602 (2005).
39. Seifert, U. Stochastic thermodynamics, fluctuation theorems and molecular machines. *Rep. Prog. Phys.* **75**, 126001 (2012).
40. Plata, C. A., Guéry-Odelin, D., Trizac, E. & Prados, A. Finite-time adiabatic processes: Derivation and speed limit. *Phys. Rev. E* **101**, 032129 (2020).
41. Martínez, I. A., Roldán, É, Dinis, L., Petrov, D. & Rica, R. A. Adiabatic processes realized with a trapped Brownian particle. *Phys. Rev. Lett.* **114**, 120601 (2015).
42. Roldán, É., Martínez, I. A., Dinis, L. & Rica, R. A. Measuring kinetic energy changes in the mesoscale with low acquisition rates. *Appl. Phys. Lett.* **104**, 234103 (2014).
43. Li, T., Kheifets, S., Medellin, D. & Raizen, M. G. Measurement of the instantaneous velocity of a brownian particle. *Science* **328**, 1673 (2010).
44. Huang, R. et al. Direct observation of the full transition from ballistic to diffusive brownian motion in a liquid. *Nat. Phys.* **7**, 576 (2011).
45. Kheifets, S., Simha, A., Melin, K., Li, T. & Raizen, M. G. Observation of brownian motion in liquids at short times: instantaneous velocity and memory loss. *Science* **343**, 1493 (2014).
46. Brandner, K., Saito, K. & Seifert, U. Thermodynamics of micro-and nano-systems driven by periodic temperature variations. *Phys. Rev. X* **5**, 031019 (2015).
47. Gronchi, G. & Puglisi, A. Optimization of an active heat engine. *Phys. Rev. E* **103**, 052134 (2021).
48. Gal, A. & Raz, O. Precooling strategy allows exponentially faster heating. *Phys. Rev. Lett.* **124**, 060602 (2020).
49. Patrón, A., Prados, A. & Plata, C. A. Thermal brachistochrone for harmonically confined brownian particles. *Eur. Phys. J.* **137**, 1 (2022).

Acknowledgements

The authors acknowledge the Korea Institute for Advanced Study for providing computing resources (KIAS Center for Advanced Computation Linux Cluster System). This research was supported by NRF Grants No. 2017R1D1A1B06035497 (H.P.), and individual KIAS Grants No. PG064902 (J.S.L.), PG096601 (S. A.), and QP013602 (H.P.) at the Korea Institute for Advanced Study.

Author contributions

S.A. and J.S.L. conceived the initial idea and derived the main results. S.A. performed the numerical simulations. S.A., J.S.L., and H.P. contributed to discussions and writing the manuscript.

Competing interests
The authors declare no competing interests.

Additional information
Supplementary information The online version contains supplementary material available at https://doi.org/10.1038/s42005-026-02566-y.

Correspondence and requests for materials should be addressed to Jae Sung Lee.

Peer review information *Communications Physics* thanks Alessandro Sarracino and the other, anonymous, reviewer(s) for their contribution to the peer review of this work.